Theoretical Analysis of Vascular Regulatory Mechanisms Contributing to Retinal Blood Flow Autoregulation

Julia Arciero,[1] Alon Harris,[2] Brent Siesky,[2] Annahita Amireskandari,[2] Victoria Gershuny,[3] Aaron Pickrell,[4] and Giovanna Guidoboni[1]

[1]Department of Mathematical Sciences, Indiana University-Purdue University Indianapolis, Indianapolis, Indiana
[2]Eugene and Marilyn Glick Eye Institute and Indiana University School of Medicine, Indianapolis, Indiana
[3]Department of Mathematics, University of Colorado at Boulder, Boulder, Colorado
[4]St. George's University School of Medicine, Great River, New York

Correspondence: Julia Arciero, Department of Mathematical Sciences, Indiana University-Purdue University Indianapolis, Indianapolis, IN 46202; jarciero@math.iupui.edu

Submitted: December 21, 2012
Accepted: June 18, 2013

Citation: Arciero J, Harris A, Siesky B, et al. Theoretical analysis of vascular regulatory mechanisms contributing to retinal blood flow autoregulation. *Invest Ophthalmol Vis Sci*. 2013;54:5584–5593. DOI:10.1167/iovs.12-11543

Purpose. To study whether impaired retinal autoregulation is a risk factor for glaucoma, the relationship between vascular regulatory mechanisms and glaucoma progression needs to be investigated. In this study, a vascular wall mechanics model is used to predict the relative importance of regulatory mechanisms in achieving retinal autoregulation.

Methods. Resistance vessels are assumed to respond to changes in pressure, shear stress, carbon dioxide (CO_2), and the downstream metabolic state communicated via conducted responses. Model parameters governing wall tension are fit to pressure and diameter data from porcine retinal arterioles. The autoregulation pressure range for control and elevated levels of IOP is predicted.

Results. The factor by which flow changes as the blood pressure exiting the central retinal artery is varied between 28 and 40 mm Hg is used to indicate the degree of autoregulation (1 indicates perfect autoregulation). In the presence of only the myogenic response mechanism, the factor is 2.06. In the presence of the myogenic and CO_2 responses, the factor is 1.22. The combination of myogenic, shear, CO_2, and metabolic responses yields the best autoregulation (factor of 1.10).

Conclusions. Model results are compared with flow and pressure data from multiple patient studies, and the combined effects of the metabolic and CO_2 responses are predicted to be critical for achieving retinal autoregulation. When IOP is elevated, the model predicts a decrease in the autoregulation range toward low perfusion pressure, which is consistent with observations that glaucoma is associated with decreased perfusion pressure.

Keywords: autoregulation, glaucoma, retina, blood flow regulation, metabolic response, myogenic response

Glaucoma is the second leading cause of blindness worldwide[1] and is characterized by the degeneration of the optic nerve and loss of retinal ganglion cells, leading to progressive, irreversible vision loss. While elevated IOP has been identified as an important risk factor for the disease, data from the Early Manifest Glaucoma Trial and other studies suggest that factors such as disc hemorrhage,[2–4] exfoliation, low systolic perfusion pressure, thinner corneas, and a history of cardiovascular disease[2] may also contribute to the development and progression of glaucoma. Clinical observations have indicated significant correlations between impaired vascular function and glaucomatous damage,[2,5–9] and imaging studies have indicated impaired ocular blood flow as an independent risk factor for glaucomatous damage and progression.[10–17] However, these correlations and observations cannot determine whether hemodynamic alterations are the cause or result of optic nerve damage and retinal cell loss. As a first step in resolving this controversy, the present study aims to develop a mechanistic model of blood flow control in the retina that could later be used to assess whether impaired control of flow leads to tissue hypoxia and cell death when IOP is at control or elevated levels.

Vascular beds exhibit an intrinsic ability to maintain relatively constant blood flow despite changes in pressure while meeting the metabolic demands of the tissue. This process, known as autoregulation, is achieved by appropriate changes in arteriolar smooth muscle tone that cause vessels to dilate or constrict in response to pressure (myogenic response),[18] shear stress on the endothelial lining of vessels (shear-dependent response),[19–21] metabolite concentrations in vessels and/or tissue (metabolic or conducted response),[22–26] local tissue partial pressure of carbon dioxide (PCO_2) or pH levels (carbon dioxide response),[27] and neural stimuli[28,29] (see details in the Supplementary Material). Autoregulation in the retina has been attributed to the combination of some of these mechanisms. In isolated bovine and porcine retinal arterioles, myogenic tone was observed to increase as intravascular pressure was increased from 10 to 60 mm Hg.[20,30] Wall shear rate and blood viscosity were measured in human retina using retinal laser Doppler velocimetry and cone-plate viscometry,[21] and wall shear stress was found to be approximately twice as high in arterioles as in venules.[21] Conducted responses have been observed to be initiated in venules and trigger vasodilation of upstream arterioles[31,32] in multiple tissues. Alm and Bill[33]

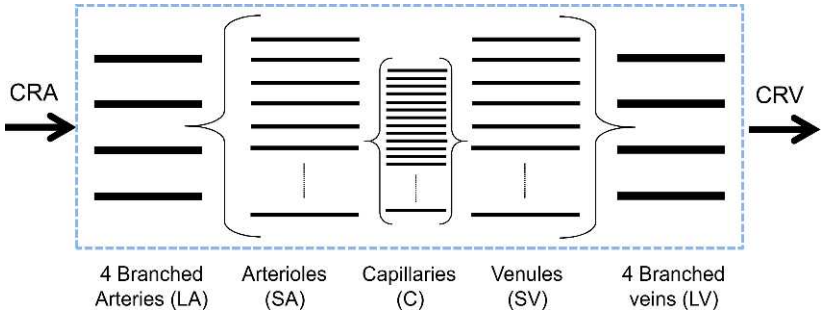

FIGURE 1. Representative segment model. The retinal vasculature is represented by five compartments downstream of the CRA and upstream of the central retinal vein (CRV). The *blue dotted line* indicates the compartments considered in this model. The vessels in the LA and SA compartments are assumed to be vasoactive, and the remaining compartments are fixed resistances.

showed retinal arteriole vasodilation in cats in response to increased $PaCO_2$. Several other metabolites, including a retinal relaxing factor,[34] may alter vascular resistance,[28] but these are not highlighted in this study since experimental evidence is limited. The inner retina is not innervated, and thus sympathetic nervous system effects are not included in this model for the retinal vascular bed.

Very few theoretical models have been developed to study hemodynamics in the retina.[35] Takahashi et al.[36] developed a mathematical model of the hemodynamic behavior in a microvascular network of the human retina that assumes a dichotomous symmetric branching vascular network. A more realistic image-based network model of a murine retinal vasculature was used to show that the distribution of the blood hematocrit in the retinal network is extremely nonuniform.[37] Neither of these models accounted for blood flow autoregulation or the effects of IOP on the system.

In the current study, we aim to combine, for the first time, a network model of retinal hemodynamics with the effect of IOP and blood flow regulation. An established vascular wall mechanics model[38] is adapted to evaluate regulatory mechanisms that have been shown experimentally[20,21,30,33] to contribute to autoregulation in the retina. Terms for myogenic, shear, conducted metabolic, and carbon dioxide responses are defined in a function that dictates the tone (and diameter) of arterioles. Parameter values and functional forms for each mechanism are determined, when possible, from experimental data[20,30,33,39] or estimated according to clinical observations. The model is used to simulate a situation in which autoregulation functions properly; then, various mechanisms are removed to determine the effect of impaired autoregulatory mechanisms on blood flow. These simulations are repeated for an elevated level of IOP to examine the effects of IOP on blood flow autoregulation.

METHODS

Representative Segment Model

To evaluate how myogenic, shear-dependent, metabolic, and carbon dioxide mechanisms combine to achieve blood flow autoregulation in the retina, a simplified model, known as a representative segment model (developed previously[23]), is used in which vessel compartments are connected in series and contain a set of identical, parallel-arranged segments that experience the same hemodynamic and metabolic conditions. The representative segment model of the retina presented in this study is used to evaluate flow downstream of the central retinal artery (CRA) through five representative segments: large arterioles (LA; the four vessels that branch from the CRA), small arterioles (SA), capillaries (C), small venules (SV), and large venules (LV; the four vessels that drain into the central retinal vein). Figure 1 provides a schematic of the vessel network used in this study. The pathway is assumed to be symmetric with respect to vessel length (L) and number (n) in corresponding arteriolar and venous compartments; flow resistance (R) is calculated according to Poiseuille's Law:

$$R = \frac{128L\mu}{\pi n D^4} \quad (1)$$

where μ is the blood viscosity and D is the vessel diameter. The vessels primarily responsible for regulating blood flow are resistance vessels with diameters smaller than 150 μm. Therefore, the large and small arterioles are assumed to be vasoactive and the remaining compartments are considered to be fixed resistances. Flow (Q) and the change in pressure (ΔP) are related by:

$$Q = \frac{\Delta P}{R}. \quad (2)$$

Ocular Perfusion Pressure

The model is used to predict blood flow along the defined vascular pathway as the incoming arterial pressure to the network, denoted by P_a, is varied. Ocular perfusion pressure (OPP) is defined as the difference between ocular arterial pressure and IOP[40] and is approximated by:

$$OPP = \frac{2}{3}MAP - IOP \quad (3)$$

where MAP is the mean arterial pressure in the brachial artery and is approximately 90 mm Hg under normal conditions. Since the first term of Equation 3 approximates the average blood pressure entering the ophthalmic artery, we define a separate quantity for the OPP of the retina, OPP_{ret}, that corresponds to perfusion pressure of the retinal vascular network:

$$OPP_{ret} = P_a - IOP. \quad (4)$$

Under normal conditions, $P_a = 40$ mm Hg, which is the approximate pressure of blood exiting the CRA calculated previously by Carichino et al.[41] Their calculation accounted for the compression exerted by the lamina cribrosa on the CRA due to IOP, retrolaminar tissue pressure, and scleral tension. Takahashi et al.[36] used a nearly equal value (38.9 mm Hg) for this pressure, which they estimated by considering the hydrostatic and frictional pressure losses from the aorta to the CRA. Since the intraocular veins experience a significant

Investigative Ophthalmology & Visual Science

Table 1. Parameter Values Defining Arteriolar Activation and Diameter

Parameter Value	Large Arteriole	Small Arteriole
C_{myo}, cm/dyn	0.0092	0.025
C_{shear}, cm^2/dyn	0.0258	0.0258
C_{meta}, μM/cm	200	200
C_{CO2}, 1/mm Hg	8e-4	1.31e-4
C"$_{tone}$	3.28	4.62
C_{pass}, dyn/cm	361.48	197.01
C'$_{pass}$	53.69	17.60
C_{act}, dyn/cm	2114.2	3089.6
C'$_{act}$	0.93	1.02
C"$_{act}$	0.11	0.20
D_0, μm	135.59	73.9

C_{pass} and C'$_{pass}$, passive tension strength and sensitivity, respectively; C_{act}, C'$_{act}$, C"$_{act}$, maximally active vascular smooth muscle peak tension, length dependence, and tension range, respectively; D_0, passive reference vessel diameter.

compressing force due to IOP, the pressure in the veins just before exiting the eye must equal or exceed the IOP, otherwise they will collapse.[42] Therefore, the venous pressure at the downstream end of the vascular network is assumed to be equal to IOP. As evident from Equation 4, OPP_{ret} can be altered by variations in P_a or IOP. Such variations correspond to changes in OPP that occur each day due to stress- or exercise-induced elevations in MAP, nocturnal reductions in arterial pressure, and diurnal variations in IOP.[43] In this study, P_a will be increased from 16 to 64 mm Hg while IOP is held constant at a control (15 mm Hg) or elevated (25 mm Hg)[44,45] level.

Arteriolar Diameter and Activation

A mechanical model of resistance vessel walls is used to assess changes in vessel diameter and vascular smooth muscle tone as P_a and/or IOP is varied. Total circumferential wall tension, T_{total}, generated in the resistance vessels (large and small arterioles) is described by a previously developed model[23,38]:

$$T_{total} = T_{passive} + AT_{active}^{max} \quad (5)$$

where A is vascular smooth muscle tone (activation):

$$A = \frac{1}{1 + exp(-S_{tone})}. \quad (6)$$

In Equation 5, passive tension, $T_{passive}$, represents the wall tension generated by the structural components of the vessel wall, and T_{active}^{max} is the maximum degree of active wall tension that can be generated in response to maximal constriction of the vascular smooth muscle cells (see the Supplementary Material for details). Parameters for the passive and maximally active tension functions are fit in a least squares sense to data from autoregulation studies in retina[30] and brain[39] and are listed in Table 1. The product of activation, which is assumed to be a value between 0 and 1, and T_{active}^{max} defines the active tension generated by the smooth muscle in the vessel wall. The smooth muscle activation defined in Equation 6 depends on a stimulus function, S_{tone}, which dictates changes in smooth muscle tone according to a linear combination of regulatory mechanisms:

$$S_{tone} = C_{myo}T - C_{shear}\tau - C_{meta}S_{CR} - C_{CO2}S_{CO2} + C''_{tone}. \quad (7)$$

This function is adapted from References 23 and 38 and includes the action by myogenic (term 1), shear dependent (term 2), conducted metabolic (term 3), and local carbon dioxide responses (term 4). Although not in the previous models, a carbon dioxide mechanism is explicitly included here because tissue levels of PCO_2 and pH have been shown to be significant factors in retinal and brain autoregulation.[26,27,46,47]

Model Calculations for Components of S_{tone}

In Equation 7, the values for wall tension (T), wall shear stress (τ), the conducted response signal (S_{CR}), and the carbon dioxide signal (S_{CO2}) are calculated using the model, and the coefficients C_{myo}, C_{shear}, C_{meta}, C_{CO2} and C''_{tone} are fit to experimental data[39,48] when possible. Vessel wall tension is approximated using the law of Laplace:

$$T = \frac{(\Delta P)D}{2} = \frac{(P - IOP)D}{2} \quad (8)$$

where ΔP is the transmural pressure across the vessel wall. Wall shear stress is proportional to flow and, according to Poiseuille's Law, is given by:

$$\tau = \frac{32\mu Q}{\pi D^3}. \quad (9)$$

S_{CR} is a red blood cell–derived conducted response signal that is initiated by the release of ATP at the downstream end of the small venule according to the saturation of the red blood cell; the signal is transmitted upstream to alter the arteriolar smooth muscle tone (see the Supplementary Material for more details). The inclusion of a carbon dioxide response mechanism is a new feature of the model. The precise mechanism by which arterioles dilate in response to lowered tissue PCO_2 is unknown, but empirical studies have shown that carbon dioxide concentrations directly alter the local tissue pH, which in turn affects the vasoconstriction of blood vessels. In this study, the carbon dioxide signal, S_{CO2}, is calculated based on the PCO_2 in the tissue (details are provided in the Supplementary Material).

Model Parameter Estimation

In Equation 7, C_{myo}, C_{shear}, C_{meta}, and C_{CO2} are weights that define the relative contributions of each mechanism to vascular tone; the positive or negative sign preceding each term corresponds to the increase or decrease in tone generated by each mechanism. C''_{tone} represents a combination of other factors, such as the retinal relaxation factor, that influences vascular tone.[34] C_{myo} is fit to data from Jeppesen et al.,[30] C_{shear} is taken directly from an autoregulation model for skeletal muscle,[38] C_{CO2} is fit to data from Wei et al.,[39] and a range of values for C_{meta} was considered since there is currently not enough experimental data to quantify this parameter. For the simulations presented in this study, a single value of C_{meta} was chosen from the range of values and is listed in Table 1 with the other parameters.

Figures 2A, 2B show the fit of the model to passive diameter data for small and large arterioles, respectively, in porcine retinal tissue.[30] The fit is obtained in a least squares sense assuming activation is zero (i.e., only passive dilation is permitted) and is used to estimate the parameters in Equation 7. Arteriolar diameter data for varied pressure values in cat brain is given at normal and elevated levels of CO_2.[39] These data are used to obtain parameters for the maximally active tension function (in Equation 13 of the Supplementary Material) as well as C_{myo} and C_{CO2} in the T passive function (see Supplementary Material). In a study by Wei et al.,[39] the diameter data is provided only as a percent

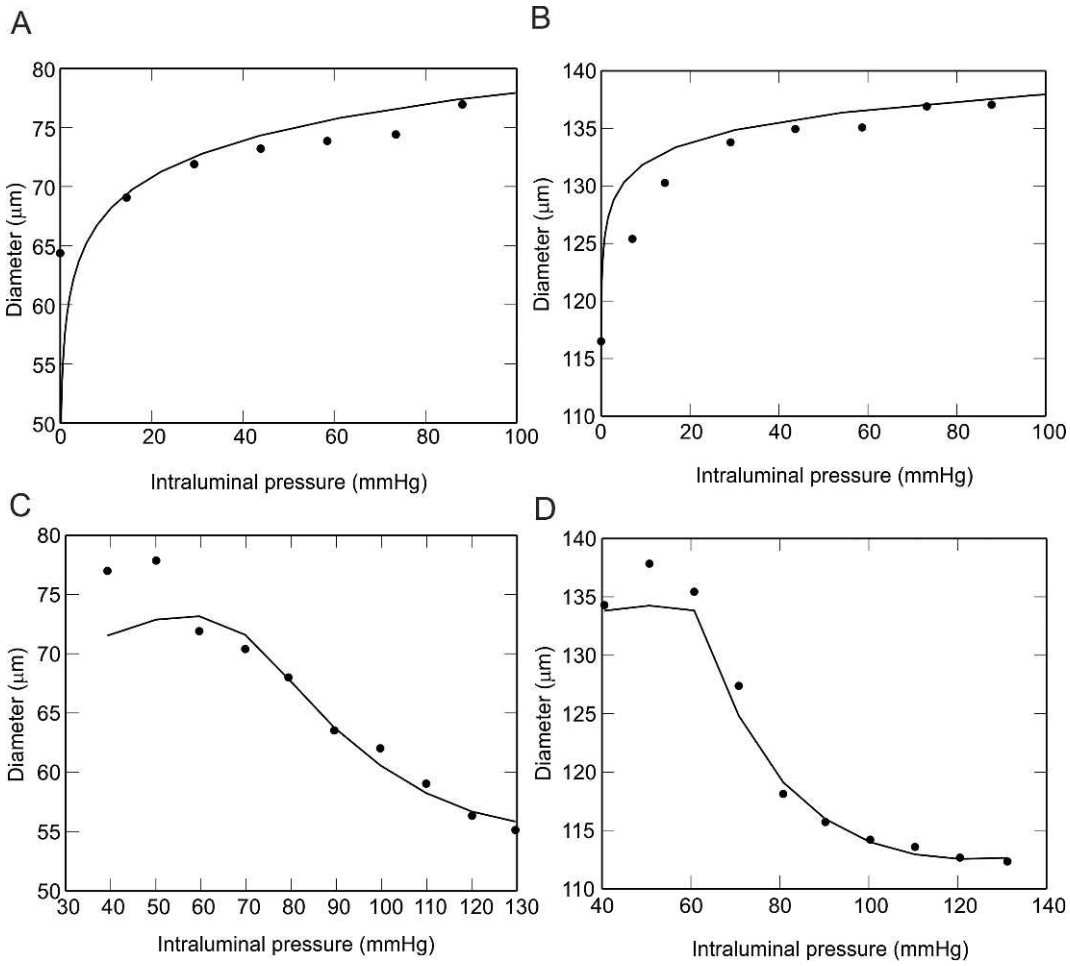

Figure 2. Parameter estimation for passive and active wall tension functions. (**A**) Diameter of small arterioles (D_{SA}) and (**B**) large arterioles (D_{LA}) as a function of arterial pressure. Model predicted values for passive diameters (*thin curve*) are compared with data from passive diameter responses (*closed circles*) in porcine retinal arterioles.[30] (**C**) Diameter of small arterioles and (**D**) large arterioles as a function of arterial pressure. Model predicted values for the active response (*thin curve*) include myogenic and carbon dioxide mechanisms and are compared with data from active diameter responses (*closed circles*) in cat brain pial arterioles.[39]

change in diameter, and thus these percentages are applied to both small and large arterioles in the present model. Parameter fits to these data are shown in Figures 2C, 2D.

Determination of Steady State Diameter and Activation

As incoming arterial pressure (P_a) is varied, arterioles show a rapid passive change in diameter followed by an active smooth muscle contraction or dilation to a new equilibrium diameter. As in a previous study,[23] this behavior is represented by a system of ordinary differential equations for D_i and A_i (i = LA, SA):

$$\begin{cases} \dfrac{dD_i}{dt} = \dfrac{1}{\tau_d}\dfrac{D_c}{T_c}(T_i - T_{total}) \\ \dfrac{dA_i}{dt} = \dfrac{1}{\tau_a}(A_{total} - A_i) \end{cases} \quad (10)$$

where $\tau_d = 1$ second and $\tau_a = 1$ minute are time constants governing the rates of passive diameter and activation changes[29,49] and D_C and T_C are control state values (see Supplementary Material) of diameter and tension, the values of which do not affect the steady state solutions of the system. Steady-state values of D and A in LA and SA are determined by integrating Equation 10 until equilibrium is reached. The values of diameter, length, number, shear stress, pressure drop, velocity, and viscosity for each representative segment are provided in Table 2 at a control (reference) state, which is defined to represent conditions in the retina that correspond to a typical level of oxygen consumption and IOP. Additional details regarding control state calculations are provided in the Supplementary Material.

Elevation in IOP

Changes in IOP affect both the transmural pressure across the vessel wall and the final venous pressure in the network, and thus a large emphasis of this study is placed on assessing how changes in IOP affect system dynamics and the generation of autoregulation. A change in IOP alters the diameter, flow, shear stress, and pressure drop in each compartment. The details of the effects of IOP on the calculation of diameter, flow, shear stress, and pressure drop are described in the Supplementary Material.

Table 2. Control State Values for Representative Segments

Description	LA	SA	C	SV	LV
Diameter, D, μm	105.0	47.2	6.0	68.5	154.9
Wall shear stress, τ, dyn/cm^2	30	30	15	10	10
Pressure drop, ΔP, mm Hg	6.25	10	5.04	2.30	1.41
No. of segments, *n*	4	40	187,890	40	4
Segment length, L, cm	0.73	0.52	0.067	0.52	0.73
Velocity, v, cm/s	1.72	0.86	0.011	0.41	0.79
Viscosity, μ, cP	2.28	2.06	10.01	2.09	2.44

Results

Model Validation

The model predicted values of blood velocity along the vascular network in the control state are compared with measured data[50–52] in Figure 3A. Velocity measures[50] were given for multiple vessel diameters, allowing for comparison with calculated velocity values in each vessel compartment of the model. The data from Riva et al.[50] were not used for any parameter estimation in this model. Several studies have also reported blood flow values measured in a few large arterioles or veins.[44,50–54] These measurements are shown in Figure 3B and are compared with the model predictions to provide additional validation of the model.

Data from population-based studies[55] include measures of the retinal arteriole-to-venous ratio (AVR), which is the ratio of the caliber of arterioles to venules. Vessel diameters were obtained by the model in the control state independently of this ratio data. The model predicted average value of $AVR = 0.72 \pm 0.05$ is consistent with the measured value of $AVR = 0.78 \pm 0.10$ in the human retina,[55] thereby providing additional evidence of the consistency of the model with measured data.

Investigation of Autoregulation Mechanisms

Figure 4 shows the changes in oxygen saturation and blood content of carbon dioxide with distance along the vascular pathway for three levels of P_a: 32, 40, and 64 mm Hg. Oxygen consumption is assumed constant at 1 cm^{3}O$_2$/100 cm^3/min. The greatest drop in oxygen saturation (Fig. 4A) is predicted to occur across the capillaries. Saturation remains constant in the small and large venules since oxygen exchange by these segments is neglected. In Figure 4B, carbon dioxide is predicted to increase with distance along the vascular network since the metabolic rate of CO_2 is proportional to that of oxygen by a negative factor.[56]

Figure 5A shows the model predictions of normalized blood flow (normalized with respect to flow at $P_a = 40$ mm Hg) as a function of incoming arterial pressure, P_a, with various autoregulation mechanisms assumed to be active or inactive. P_a is varied between 16 and 64 mm Hg and IOP is held constant at a control level of IOP = 15 mm Hg. Removing or adding mechanisms from the model allows for a theoretical assessment of impaired or ineffective mechanisms on blood flow autoregulation. To quantify this impairment, the factor by which flow changes as P_a is varied between 28 and 40 mm Hg is used to indicate the degree of autoregulation and is denoted AR_f. In particular, the factor is given by:

$$AR_f = \frac{Q_{40}}{Q_{28}} \quad (11)$$

where Q_{40} is the flow when $P_a = 40$ mm Hg and Q_{28} is the flow when $P_a = 28$ mm Hg. This approximate 40% increase in blood pressure is used since previous reports have stated that autoregulation was effective up to a 40% rise in blood pressure.[44] A factor of $AR_f = 1$ indicates perfect autoregulation.

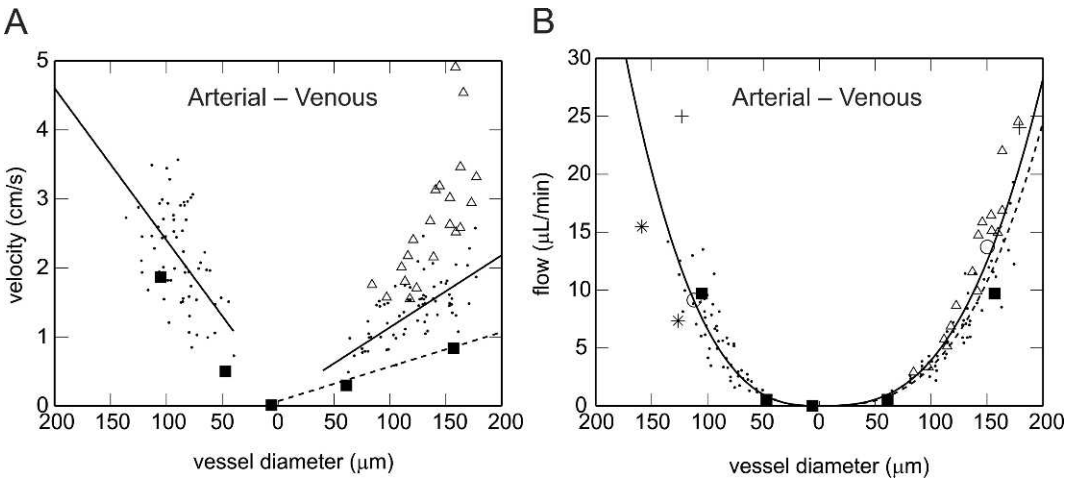

Figure 3. **(A)** Comparison of model predicted velocity values (*black squares*) with experimental measures (*black dots*,[50] *open triangles*,[51] *dashed line*[52]) for different-sized vessels. The *solid line* corresponds to the best fit line to the experimental data, as determined in a study by Riva et al.[50] **(B)** Rate of blood flow (Q) as a function of vessel diameter for arterioles and venules. *Solid curve* is the power curve fit to the data points from arteries and veins[50] (*black dots*). Riva et al.[50] found that $Q_A = 2e-5D^{2.76}$ and $Q_V = 8.25e-6D^{2.84}$ where diameter is in micrometers. Additional measures of blood flow for different vessel sizes are included from Feke et al.[53] (*plusses*), Dumskyj et al.[44] (*open circles*), Rassam et al.[54] (*asterisks*), Garcia Jr et al.[51] (*open triangles*), and Grunwald et al.[52] (*dashed line*). *Black squares* correspond to model predicted flow values in the control state.

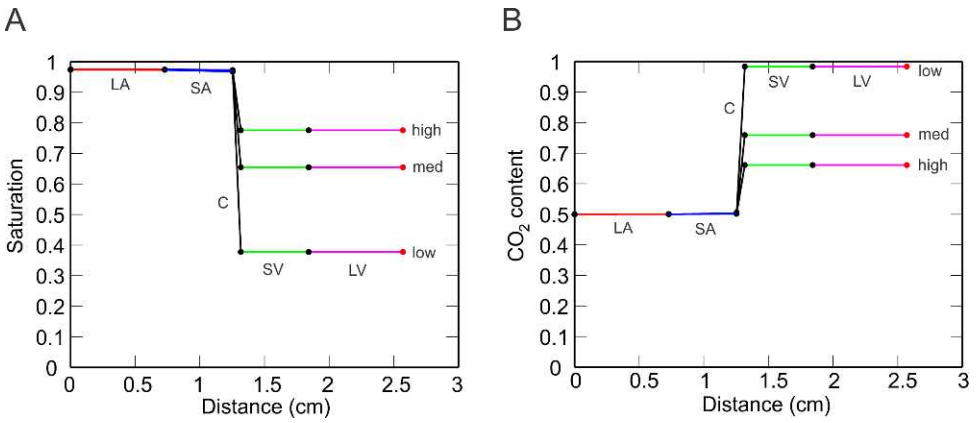

FIGURE 4. (**A**) Decline of oxygen saturation along the vascular network (compartments are colored and labeled) for incoming pressures of $P_a = 32$ (low), 40 (medium), and 64 mm Hg (high). (**B**) Increase in carbon dioxide content of blood along the vascular network. Pressures as in (**A**).

The dashed black line in Figure 5A gives the predicted passive increase in flow with pressure when no mechanisms are active. In the presence of only the myogenic response mechanism (red curve), the model predicts a poor degree of autoregulation ($AR_f = 2.06$). Including the shear response (green curve) does not improve the predicted autoregulation of blood flow ($AR_f = 2.15$). A local carbon dioxide response combined with the myogenic and shear responses (black curve) yields improved autoregulation ($AR_f = 1.24$), and the addition of the conducted metabolic response provides the best degree of autoregulation ($AR_f = 1.10$). Table 3 provides additional combinations of the response mechanisms in order to illustrate which mechanisms are predicted to be most important in obtaining constant blood flow over a range of arterial pressures. Figures 5B, 5C show the diameter constriction necessary in the LA and SA compartments to achieve autoregulation.

Effect of IOP on Autoregulation

Assuming that all four regulatory mechanisms are functioning, the model is compared with clinical data[44,57–59] and is used to evaluate the effect of increased IOP on blood flow autoregulation (Fig. 6). In Figure 6A, clinical measures from healthy subjects or from glaucoma patients whose autoregulation was reported to be normal are plotted along with the model-predicted autoregulation curve for a control level of IOP. The model predicts very small changes in flows over the observed pressure differences. Most of the data points fall at or around the model predicted curve. One of the included data sets[58] (diamonds in Fig. 6A), however, is from glaucoma patients who have not been treated with Brimonidine and therefore exhibit a limited ability to autoregulate while reclining. This data set was included to provide some preliminary evidence that the model correctly reflects the boundary of the autoregulation range. As shown in Figure 6B, the autoregulation curve for a control level of IOP = 15 mm Hg (blue curve) is predicted to shift rightward if IOP is elevated to 25 mm Hg (red curve). The length of the autoregulation range (i.e., pressures for which the autoregulation curve remains nearly flat) is conserved despite increases in IOP (see Fig. 6C); however, autoregulation fails to operate over its expected pressure range when IOP is elevated. In particular, the autoregulation factor of $AR_f = 1.10$ for normal IOP increases to $AR_f = 4.65$ for elevated IOP as P_a increases from 28 to 40 mm Hg.

DISCUSSION

Elevated IOP has been established as a major risk factor for the development and progression of glaucoma and is currently the only treatable risk factor for the disease. However, several observations, including the progression of glaucomatous damage even when IOP is lowered to within target levels

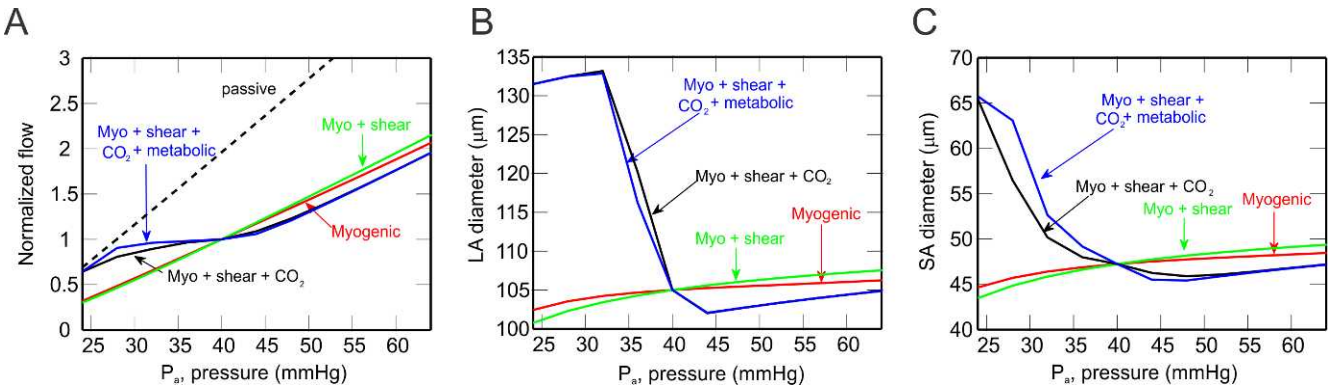

FIGURE 5. (**A**) Change in blood flow as pressure, P_a, is increased, providing a measure of the degree of blood flow autoregulation. P_a is defined as the pressure at the downstream end of the CRA. The *dashed line* represents a passive vessel response when no regulatory mechanisms are active. Individual and combined roles of myogenic, shear, conducted metabolic, and carbon dioxide mechanisms on autoregulation are evaluated at a control level of $IOP = 15$ mm Hg. (**B**) Corresponding changes in LA diameter with pressure. (**C**) Corresponding changes in SA diameter with pressure.

Table 3. Factors by Which Blood Flow Increases With Pressure Changes From 28 to 40 mm Hg

Active Mechanisms	Autoregulation Factor, AR_f
Myogenic	2.06
Shear	2.29
CO_2	1.23
Metabolic	1.14
Myogenic and shear	2.15
Myogenic and CO_2	1.22
Myogenic and metabolic	1.13
Myogenic, shear, and CO_2	1.24
Myogenic, shear, CO_2, and metabolic	1.10

and the role of racial variations in the incidence of glaucoma, suggest that other factors also play a critical role in the development of this disease.[60] The contribution of impaired blood flow autoregulation to blood flow insufficiency has been proposed as an additional risk factor for glaucoma.[60] The goal of the current study was to assess the regulatory mechanisms that contribute to autoregulation in the retina and to simulate conditions under which autoregulation may become impaired. This model provides an initial step in the ultimate goal of elucidating how impaired autoregulation may be related to the retinal ganglion cell death characteristic of glaucoma.

Model Validation

Given the simplifying assumptions of any theoretical model, it is necessary to compare model predictions with clinical or experimental data to verify model performance and to provide confidence that the model predictions can provide valuable insight into diseases such as glaucoma. Figure 6A compares clinical data to a model predicted autoregulation curve, and Figure 3 provides evidence that the model predicted velocities and flows lie in the same range as clinically measured quantities. In Figure 3B, there are a few slight discrepancies among the clinical data. For example, both Feke et al.[53] and Riva et al.[50] provide measures of average retinal blood flow in humans using laser Doppler techniques, although their measures of total arterial and venous flow rates vary by over a factor of 2 in some cases. Feke et al.[53] showed that flow indeed varied with the fourth power of diameter (i.e., consistent with Poiseuille's Law), whereas Riva et al.[50] reported a power of approximately 2.8. Differences in their respective experimental methodologies may explain these discrepancies. Moreover, Riva et al.[50] included flow measurements for vessels with diameters significantly smaller than those measured by Feke et al.[53], and in smaller vessels, $\Delta P/\Delta L$ may depend on vessel diameter.

None of the clinical measures shown in Figure 3 were used to estimate any of the model parameters; these measures were used solely for comparison purposes. Given the simplified geometry of the model presented here (i.e., the representative segment model), the general consistency of flow and velocity predicted by the model (depicted in Fig. 3) with flow and velocity measures from several studies[44,50,53,54] provides evidence that the model assumptions and mechanisms are accurate and appropriate.

Investigation of Autoregulation Mechanisms

Retinal blood flow autoregulation is achieved by altering the tone of arteriolar smooth muscle cells according to myogenic, shear-dependent, metabolic, and carbon dioxide mechanisms. Anderson[61] hypothesized that tissue ischemia occurs either because the capacity for autoregulation is exceeded or the mechanisms of autoregulation are defective. The model developed in this study can be used to test such hypotheses. The purpose of autoregulation is to maintain blood flow despite a significant change in pressure (e.g., if MAP is low or IOP is high). This model predicts that autoregulation is severely compromised if the metabolic or carbon dioxide mechanisms are not functioning properly (Fig. 5).

The model also predicts that the myogenic response does not contribute significantly to autoregulation in the retina. It is important to note that the myogenic response is highly nonlinear with respect to vessel diameter and that the myogenic response may not be very effective in this pressure regime because wall tensions are too low. Understanding under what conditions the myogenic mechanism may become more or less responsive could help in continuing to elucidate the most important mechanisms for autoregulation.

Effect of IOP on Autoregulation

IOP creates a challenge to retinal blood flow by raising the venous pressure at the downstream end of the retinal vasculature, which corresponds to a decreased perfusion pressure through the retinal vasculature.[61] As IOP rises, venous pressure also rises in order to keep the veins distended. This is mostly due to the constriction of central retinal vessels

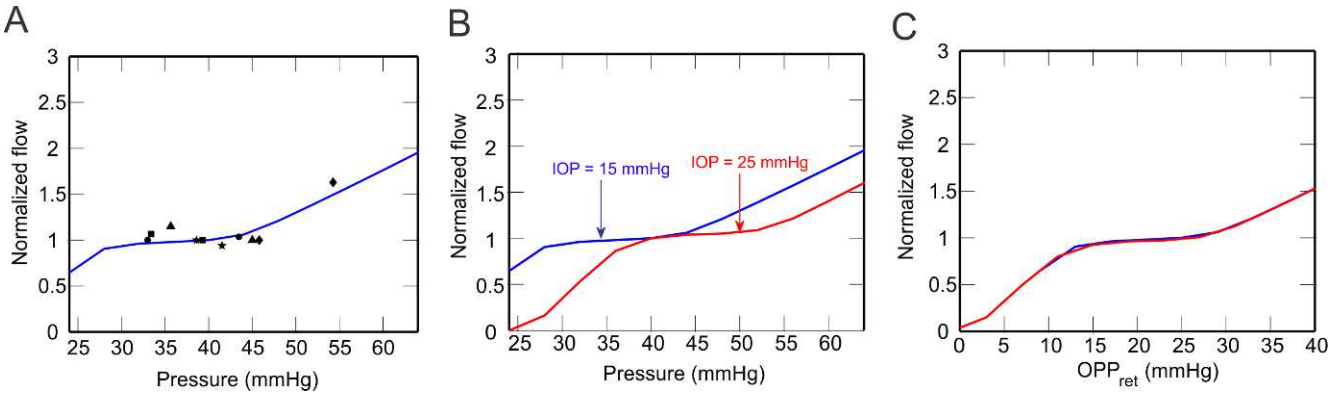

Figure 6. Model predicted autoregulation curves for $IOP = 15$ mm Hg (control) and $IOP = 25$ mm Hg (elevated). (**A**) For $IOP = 15$ mm Hg, the model predicted autoregulation curve (*solid curve*) is plotted with clinical data obtained from Feke and Pasquale.[59] (*squares* and *triangles*), Dumskyj et al.[44] (*circles*), Feke et al.[58] (*diamonds*), and Grunwald[57] (*stars*). (**B**) Normalized flow plotted as a function of P_a for $IOP = 15$ mm Hg (*blue*) and $IOP = 25$ mm Hg (*red*). (**C**) Normalized flow plotted as a function of OPP_{ret}. Colors as in (**B**).

by the IOP-induced deformation of the lamina cribrosa.[41] Importantly, since IOP is normally higher than extraocular venous pressure, perfusion pressure in the eye (even with normal IOP) is already less than in other tissues and becomes even further diminished if IOP is elevated.[61]

The model predicts that autoregulation fails to operate over its expected pressure range if IOP is increased, indicating that autoregulation is impaired at low perfusion pressure. This result provides a potential explanation for why impaired autoregulation is hypothesized to be a contributing factor to glaucoma progression.[43] An important goal of these simulations is to determine the maximum value of IOP and minimum value of ocular perfusion pressure at which autoregulation is efficient.[62] Kiel and van Heuven[63] showed that choroidal autoregulation was most effective when MAP was varied and IOP was not controlled. Thus, the effects of MAP and IOP alterations on retinal autoregulation should be investigated using both theoretical and clinical approaches. To complicate matters, the exact level of IOP that can be tolerated may differ among patients.[61] Moreover, glaucoma is known to occur despite IOP being at control values. In fact, studies in multiple populations indicate that certain healthy individuals possess a very narrow pressure autoregulatory plateau, potentially making these patients more susceptible to retinal ischemia and disease.[43] As demonstrated by the model, even if IOP is at a control level, defective mechanisms can significantly impair autoregulation.

Limitations of the Present Model

The present model involves some simplifications. The four mechanisms included in this model do not represent all known mechanisms of autoregulation in the retina. The model is also limited by the amount of available experimental and clinical data on the role of shear responses and conducted metabolic responses in the retina and on the responses of vessels to different mechanisms in different-sized vessels. Thus, some model parameters cannot be determined and instead are estimated or varied. Currently, the model is simulated using a compartmental approach in which vessels are assumed to be identical in each compartment; model extensions will allow for a heterogeneous network to account for the actual spatial distribution of vessels. The present model considers the entire venous side as a fixed resistance. However, venous diameters may be influenced by metabolic, endothelial, and pressure changes, and thus a similar combined active and passive component governing the changes in arteriolar diameters should be applied to venular diameters. Finally, the model predictions are found at steady state; expanding the model to investigate time-dependent mechanisms and time-dependent changes in pressure will provide insight into the effects of systolic and diastolic pressures on flow autoregulation in the retina.

Conclusions

The theoretical model presented in this study provides a framework that can be extended or altered to incorporate additional mechanisms of autoregulation. For example, capillaries, which are normally assumed to be passive resistors, may contribute to the regulation of flow in the retina due to the contraction or dilation of pericytes, which are cells surrounding the capillary that function similarly to vascular smooth muscle cells.[64] Pericytes are more abundant in the retina than most tissues in the body and have been shown to respond to increased levels of lactate production in the retina.[25] The model could be used to assess the effects of this mechanism by allowing the capillary compartment to be vasoactive.

Perfusion instability may also play a role in glaucoma development. It is well-known that circadian rhythms are important for maintaining homeostasis in the body; it would be interesting to adapt the current theoretical model to evaluate the effects of circadian rhythms on systemic blood pressure, ocular perfusion pressure, and ocular blood flow.[65] It is hypothesized that abnormal vascular reactions to a reduction in pressure or increase in IOP during nonwaking hours may contribute to perfusion instability and thus the progression of glaucoma.

The current model shows that the metabolic and carbon dioxide responses are critical for autoregulation. The ability to autoregulate is reduced by 13% if the conducted metabolic response is impaired and is reduced by 95% if both the metabolic and carbon dioxide responses are impaired. The model also predicts that autoregulation is impaired at decreased perfusion pressures due to elevated IOP; in particular, the lower limit of the pressure range of autoregulation is increased by approximately 42% when IOP is increased from 15 to 25 mm Hg, providing evidence for why impaired autoregulation is hypothesized to be a contributing factor to OAG progression. Ultimately, isolating and quantifying the relevance of regulatory mechanisms and IOP on blood flow autoregulation using theoretical modeling can provide important insight that may not be obtained from clinical studies in which isolating mechanisms and behaviors is nearly impossible.

Acknowledgments

Supported by National Science Foundation Grants DMS-1224195 (JA, GG) and DMS-1134731 (GG), the Indiana University Collaborative Research Grant of the Office of the Vice President for Research (GG, AH), and National Institutes of Health Grant 1R21EY022101-01A1 (AH).

Disclosure: **J. Arciero**, None; **A. Harris**, None; **B. Siesky**, None; **A. Amireskandari**, None; **V. Gershuny**, None; **A. Pickrell**, None; **G. Guidoboni**, None

References

1. Leske MC. Open-angle glaucoma—an epidemiologic overview. *Ophthalmic Epidemiol*. 2007;14:166–172.
2. Leske MC, Heijl A, Hyman L, Bengtsson B, Dong L, Yang Z. Predictors of long-term progression in the early manifest glaucoma trial. *Ophthalmology*. 2007;114:1965–1972.
3. Bengtsson B, Leske MC, Yang Z, Heijl A. Disc hemorrhages and treatment in the early manifest glaucoma trial. *Ophthalmology*. 2008;115:2044–2048.
4. De Moraes CG, Juthani VJ, Liebmann JM, et al. Risk factors for visual field progression in treated glaucoma. *Arch Ophthalmol*. 2011;129:562–568.
5. Hulsman CA, Vingerling JR, Hofman A, Witteman JC, de Jong PT. Blood pressure, arterial stiffness, and open-angle glaucoma: the Rotterdam study. *Arch Ophthalmol*. 2007;125:805–812.
6. Bonomi L, Marchini G, Marraffa M, Bernardi P, Morbio R, Varotto A. Vascular risk factors for primary open angle glaucoma: the Egna-Neumarkt Study. *Ophthalmology*. 2000; 107:1287–1293.
7. Topouzis F, Wilson MR, Harris A, et al. Association of open-angle glaucoma with perfusion pressure status in the Thessaloniki Eye Study. *Am J Ophthalmol*. 2013;155:843–851. e841.
8. Kashiwagi K, Tsumura T, Ishii H, Ijiri H, Tamura K, Tsukahara S. Circadian rhythm of autonomic nervous function in patients with normal-tension glaucoma compared with normal subjects using ambulatory electrocardiography. *J Glaucoma*. 2000;9: 239–246.

9. Gasser P, Flammer J. Blood-cell velocity in the nailfold capillaries of patients with normal-tension and high-tension glaucoma. *Am J Ophthalmol*. 1991;111:585–588.
10. Galassi F, Sodi A, Ucci F, Renieri G, Pieri B, Baccini M. Ocular hemodynamics and glaucoma prognosis: a color Doppler imaging study. *Arch Ophthalmol*. 2003;121:1711–1715.
11. Martinez A, Sanchez M. Predictive value of colour Doppler imaging in a prospective study of visual field progression in primary open-angle glaucoma. *Acta Ophthalmol Scand*. 2005; 83:716–722.
12. Martinez A, Sanchez-Salorio M. Predictors for visual field progression and the effects of treatment with dorzolamide 2% or brinzolamide 1% each added to timolol 0.5% in primary open-angle glaucoma. *Acta Ophthalmol*. 2010;88: 541–552.
13. Evans DW, Harris A, Garrett M, Chung HS, Kagemann L. Glaucoma patients demonstrate faulty autoregulation of ocular blood flow during posture change. *Br J Ophthalmol*. 1999;83: 809–813.
14. Pillunat LE, Stodtmeister R, Wilmanns I, Christ T. Autoregulation of ocular blood flow during changes in intraocular pressure. Preliminary results. *Graefes Arch Clin Exp Ophthalmol*. 1985;223:219–223.
15. Wang L, Cull GA, Piper C, Burgoyne CF, Fortune B. Anterior and posterior optic nerve head blood flow in nonhuman primate experimental glaucoma model measured by laser speckle imaging technique and microsphere method. *Invest Ophthalmol Vis Sci*. 2012;53:8303–8309.
16. Fortune B, Choe TE, Reynaud J, et al. Deformation of the rodent optic nerve head and peripapillary structures during acute intraocular pressure elevation. *Invest Ophthalmol Vis Sci*. 2011;52:6651–6661.
17. Gardiner SK, Fortune B, Wang L, Downs JC, Burgoyne CF. Intraocular pressure magnitude and variability as predictors of rates of structural change in non-human primate experimental glaucoma. *Exp Eye Res*. 2012;103:1–8.
18. Bayliss WM. On the local reactions of the arterial wall to changes of internal pressure. *J Physiol*. 1902;28:220–231.
19. Davis MJ, Sikes PJ. Myogenic responses of isolated arterioles: test for a rate-sensitive mechanism. *Am J Physiol*. 1990;259: H1890–H1900.
20. Delaey C, Van de Voorde J. Pressure-induced myogenic responses in isolated bovine retinal arteries. *Invest Ophthalmol Vis Sci*. 2000;41:1871–1875.
21. Nagaoka T, Yoshida, A. Noninvasive evaluation of wall shear stress on retinal microcirculation in humans. *Invest Ophthalmol Vis Sci*. 2006;47:1113–1119.
22. Ellsworth ML. Red blood cell-derived ATP as a regulator of skeletal muscle perfusion. *Med Sci Sports Exerc*. 2004;36:35–41.
23. Arciero JC, Carlson BE, Secomb TW. Theoretical model of metabolic blood flow regulation: roles of ATP release by red blood cells and conducted responses. *Am J Physiol Heart Circ Physiol*. 2008;295:H1562–1571.
24. Stamler JS, Jia L, Eu JP, et al. Blood flow regulation by S-nitrosohemoglobin in the physiological oxygen gradient. *Science*. 1997;276:2034–2037.
25. Yamanishi S, Katsumura K, Kobayashi T, Puro DG. Extracellular lactate as a dynamic vasoactive signal in the rat retinal microvasculature. *Am J Physiol Heart Circ Physiol*. 2006;290: H925–934.
26. Pournaras CJ, Rungger-Brandle E, Riva CE, Hardarson SH, Stefansson E. Regulation of retinal blood flow in health and disease. *Prog Retin Eye Res*. 2008;27:284–330.
27. Kontos HA, Wei EP, Raper AJ, Patterson JL Jr. Local mechanism of CO2 action of cat pial arterioles. *Stroke*. 1977;8:226–229.
28. Schmidl D, Garhofer G, Schmetterer L. The complex interaction between ocular perfusion pressure and ocular blood flow—relevance for glaucoma. *Exp Eye Res*. 2011;93: 141–155.
29. Johnson PC. Autoregulation of blood flow. *Circ Res*. 1986;59: 483–495.
30. Jeppesen P, Aalkjaer C, Bek T. Myogenic response in isolated porcine retinal arterioles. *Curr Eye Res*. 2003;27:217–222.
31. Collins DM, McCullough WT, Ellsworth ML. Conducted vascular responses: communication across the capillary bed. *Microvasc Res*. 1998;56:43–53.
32. Ellsworth ML. The red blood cell as an oxygen sensor: what is the evidence? *Acta Physiol Scand*. 2000;168:551–559.
33. Alm A, Bill A. The oxygen supply to the retina. II. Effects of high intraocular pressure and of increased arterial carbon dioxide tension on uveal and retinal blood flow in cats. A study with radioactively labelled microspheres including flow determinations in brain and some other tissues. *Acta Physiol Scand*. 1972;84:306–319.
34. Delaey C, Van de Voorde J. Retinal arterial tone is controlled by a retinal-derived relaxing factor. *Circ Res*. 1998;83:714–720.
35. Harris A, Guidoboni G, Arciero JC, Amireskandari A, Tobe LA, Siesky BA. Ocular hemodynamics and glaucoma: the role of mathematical modeling. *Eur J Ophthalmol*. 2013;2:139–146.
36. Takahashi T, Nagaoka T, Yanagida H, et al. A mathematical model for the distribution of hemodynamic parameters in the human retinal microvascular network. *J Biorheol*. 2009;23: 77–86.
37. Ganesan P, He S, Xu H. Analysis of retinal circulation using an image-based network model of retinal vasculature. *Microvasc Res*. 2010;80:99–109.
38. Carlson BE, Arciero JC, Secomb TW. Theoretical model of blood flow autoregulation: roles of myogenic, shear-dependent, and metabolic responses. *Am J Physiol Heart Circ Physiol*. 2008;295:H1572–H1579.
39. Wei EP, Kontos HA, Patterson JL Jr. Dependence of pial arteriolar response to hypercapnia on vessel size. *Am J Physiol*. 1980;238:697–703.
40. Delaey C, Van De Voorde J. Regulatory mechanisms in the retinal and choroidal circulation. *Ophthalmic Res*. 2000;32: 249–256.
41. Carichino L, Guidoboni G, Arieli Y, Siesky BA, Harris A. Effect of lamina cribrosa deformation on hemodynamics of the central retinal artery: a mathematical model. Poster presented at: Annual Meeting of the Association for Research in Vision and Ophthalmology; May 2012; Fort Laurderdale, FL. Abstract 2838.
42. Kiel JW. *The Ocular Circulation*. San Rafael, CA: Morgan & Claypool Life Sciences; 2011;3:1–81.
43. Harris A, Ciulla TA, Chung HS, Martin B. Regulation of retinal and optic nerve blood flow. *Arch Ophthalmol*. 1998;116: 1491–1495.
44. Dumskyj MJ, Eriksen JE, Dore CJ, Kohner EM. Autoregulation in the human retinal circulation: assessment using isometric exercise, laser Doppler velocimetry, and computer-assisted image analysis. *Microvasc Res*. 1996;51:378–392.
45. Pournaras CJ, Riva CE. Retinal blood flow evaluation. *Ophthalmologica*. 2013;229:61–74.
46. Kontos HA, Raper AJ, Patterson JL. Analysis of vasoactivity of local pH, PCO2 and bicarbonate on pial vessels. *Stroke*. 1977; 8:358–360.
47. Raper AJ, Kontos HA, Patterson JL Jr. Response of pial precapillary vessels to changes in arterial carbon dioxide tension. *Circ Res*. 1971;28:518–523.
48. Sun D, Huang A, Koller A, Kaley G. Flow-dependent dilation and myogenic constriction interact to establish the resistance

Investigative Ophthalmology & Visual Science

of skeletal muscle arterioles. *Microcirculation*. 1995;2:289–295.

49. Falcone JC, Davis MJ, Meininger GA. Endothelial independence of myogenic response in isolated skeletal muscle arterioles. *Am J Physiol*. 1991;260:H130–H135.
50. Riva CE, Grunwald JE, Sinclair SH, Petrig BL. Blood velocity and volumetric flow rate in human retinal vessels. *Invest Ophthalmol Vis Sci*. 1985;26:1124–1132.
51. Garcia JP Jr, Garcia PT, Rosen RB. Retinal blood flow in the normal human eye using the canon laser blood flowmeter. *Ophthalmic Res*. 2002;34:295–299.
52. Grunwald JE, Riva CE, Baine J, Brucker AJ. Total retinal volumetric blood flow rate in diabetic patients with poor glycemic control. *Invest Ophthalmol Vis Sci*. 1992;33:356–363.
53. Feke GT, Tagawa H, Deupree DM, Goger DG, Sebag J, Weiter JJ. Blood flow in the normal human retina. *Invest Ophthalmol Vis Sci*. 1989;30:58–65.
54. Rassam SM, Patel V, Chen HC, Kohner EM. Regional retinal blood flow and vascular autoregulation. *Eye (Lond)*. 1996;10:331–337.
55. Baleanu D, Ritt M, Harazny J, Heckmann J, Schmieder RE, Michelson G. Wall-to-lumen ratio of retinal arterioles and arteriole-to-venule ratio of retinal vessels in patients with cerebrovascular damage. *Invest Ophthalmol Vis Sci*. 2009;50:4351–4359.
56. Ye GF, Moore TW, Buerk DG, Jaron D. A compartmental model for oxygen-carbon dioxide coupled transport in the microcirculation. *Ann Biomed Eng*. 1994;22:464–479.
57. Grunwald JE, DuPont J, Riva CE. Retinal haemodynamics in patients with early diabetes mellitus. *Br J Ophthalmol*. 1996;80:327–331.
58. Feke GT, Hazin R, Grosskreutz CL, Pasquale LR. Effect of brimonidine on retinal blood flow autoregulation in primary open-angle glaucoma. *J Ocul Pharmacol Ther*. 2011;27:347–352.
59. Feke GT, Pasquale LR. Retinal blood flow response to posture change in glaucoma patients compared with healthy subjects. *Ophthalmology*. 2008;115:246–252.
60. Harris A, Jonescu-Cuypers C, Martin B, Kagemann L, Zalish M, Garzozi HJ. Simultaneous management of blood flow and IOP in glaucoma. *Acta Ophthalmol Scand*. 2001;79:336–341.
61. Anderson DR. Introductory comments on blood flow autoregulation in the optic nerve head and vascular risk factors in glaucoma. *Surv Ophthalmol*. 1999;43:S5–S9.
62. Riva CE, Sinclair SH, Grunwald JE. Autoregulation of retinal circulation in response to decrease of perfusion pressure. *Invest Ophthalmol Vis Sci*. 1981;21:34–38.
63. Kiel JW, van Heuven WA. Ocular perfusion pressure and choroidal blood flow in the rabbit. *Invest Ophthalmol Vis Sci*. 1995;36:579–585.
64. Anderson DR. Glaucoma, capillaries and pericytes. 1. Blood flow regulation. *Ophthalmologica*. 1996;210:257–262.
65. Moore D, Harris A, Wudunn D, Kheradiya N, Siesky B. Dysfunctional regulation of ocular blood flow: a risk factor for glaucoma? *Clin Ophthalmol*. 2008;2:849–861.

Investigative Ophthalmology & Visual Science